ChemPubSoc Europe

DOI: 10.1002/chem.201900691

CHEMISTRY A European Journal Full Paper

Biomineralization

In Vitro Coral Biomineralization under Relevant Aragonite Supersaturation Conditions

Branka Njegić Džakula,[a] Simona Fermani,[b] Zvy Dubinsky,[c] Stefano Goffredo,[d] Giuseppe Falini,*[b] and Damir Kralj*[a]

Abstract: The biomineralization of corals occurs under conditions of high and low supersaturation with respect to aragonite, which corresponds to day- or night-time periods of their growth, respectively. Here, in vitro precipitation of aragonite in artificial seawater was investigated at a high supersaturation, allowing spontaneous nucleation and growth, as well as at low supersaturation conditions, which allowed only the crystal growth on the deliberately introduced aragonite seeds. In either chemical systems, soluble organic matrix (SOM) extracted from *Balanophyllia europaea* (light sensitive) or *Leptopsammia pruvoti* (light insensitive) was added. The analyses of the kinetic and thermodynamic data of aragonite precipitation and microscopic observations showed that, at high supersaturation, the SOMs increased the induction time, did not affect the growth rate and were incorporated within aggregates of nanoparticles. At low supersaturation, the SOMs affected the aggregation of overgrowing crystalline units and did not substantially change the growth rate. On the basis of the obtained results we can infer that at high supersaturation conditions the formation of nanoparticles, which is typically observed in the skeleton's early mineralization zone may occur, whereas at low supersaturation the overgrowth on prismatic seeds observed in the skeleton fiber zone is a predominant process. In conclusion, this research brings insight on coral skeletogenesis bridging physicochemical (supersaturation) and biological (role of SOM) models of coral biomineralization and provides a source of inspiration for the precipitation of composite materials under different conditions of supersaturation.

Introduction

The coral reef is probably the planet's most spectacular expression of biomineralization. This ecosystem is based on skeletal debris from many generations of mineralizing organisms, especially calcareous algae, foraminifera and corals, the latter providing much of the erosion-resistant framework.[1,2] Corals are classified in accordance to their association with symbiotic photosynthetic algae (i.e., zooxanthella), or according to their growth form (colonial or solitary).[1] Corals typically calcify about hundred times faster than the respective inorganic carbonate deposits on the reef and faster than most other calcifying organisms.[3] They form skeletons made of aragonite at the tissue-skeleton interface. The mineralization process occurs in a confined space, by exerting a biological control through calicoblastic epithelium over the ionic composition of a seawater-like and highly viscous medium rich in bio-synthesized organic matrix molecules (OM), which is partly entrapped within the skeleton.[4–8] The calcification process is assumed to take place as the sequential deposition of a few micrometer thick mineralizing growth layer, synchronically produced at the growing edge of the septa in two delimitated areas, the early mineralization zones (EMZ) and the fiber zones (FZ).[5,6] In the EMZ calcium carbonate ($CaCO_3$) appears as tiny granules. The EMZs produce the septal frameworks onto which other successive aragonite layers deposit, thus forming the aragonitic FZs that are actually the skeleton core. The analyses of EMZs and FZs (Figure 1) indicated that they have different chemical, mineralogical and OM composition.[7]

One specific feature of the calcification in symbiotic corals is a higher aragonitic skeleton growth during the daylight than at night.[9] This perceived disparity is associated with various, sometimes contradictory, experimental observations. Indeed, a lower aragonite saturation state was estimated during the night ($S_a = 3.2$) in the mineralization sites of *Galaxea fascicularis* (symbiotic), in comparison to day hours ($S_a = 25$).[10] *Stylophora*

[a] *Dr. B. Njegić Džakula, Dr. D. Kralj*
Laboratory for Precipitation Processes
Ruđer Bošković Institute, P.O. Box 180
10002 Zagreb (Croatia)
E-mail: kralj@irb.hr

[b] *Dr. S. Fermani, Prof. G. Falini*
Department of Chemistry "Giacomo Ciamician"
Alma Mater Studiorum—Universitá di Bologna
Via Selmi 2, 40126 Bologna (Italy)
E-mail: giuseppe.falini@unibo.it

[c] *Prof. Z. Dubinsky*
The Mina & Everard Goodman Faculty of Life Sciences
Bar-Ilan University, Ramat-Gan 5290002 (Israel)

[d] *Prof. S. Goffredo*
Department of Biological, Geological and Environmental Sciences
Alma Mater Studiorum—Università di Bologna
Via Selmi 3, 40126 Bologna (Italy)

Supporting information and the ORCID identification number(s) for the author(s) of this article can be found under: https://doi.org/10.1002/chem.201900691.

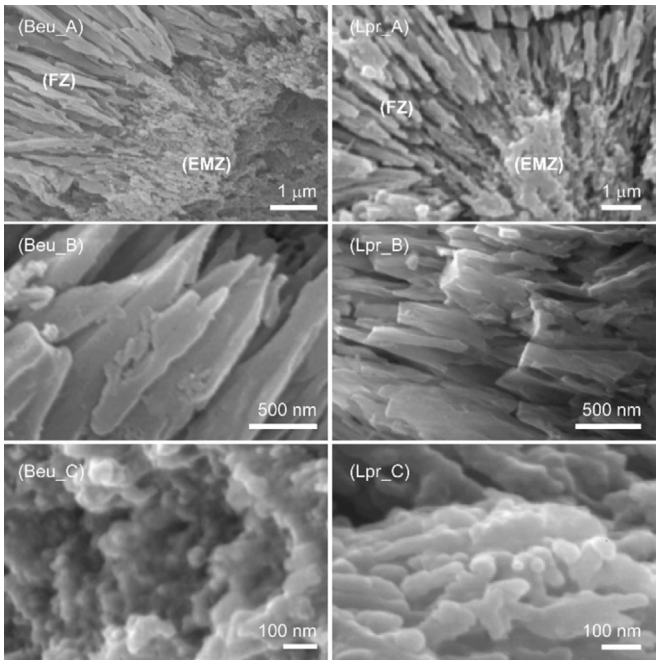

Figure 1. Scanning electron microscopy images of cross sections of septum skeletons from *B. europaea* (Beu) and *L. pruvoti* (Lpr). A) Images in which the early mineralization zone (EMZ) and the fiber zone (FZ) are visible. B) Images of the fiber zone. C) Images of the early mineralization zone.

pistillata (symbiotic) shows calcification rates constant during the day and the night with a 2.6-fold difference between day and night.

This light-enhanced calcification process has been justified by the assumption that (1) the photosynthesis increases the pH in the coelenteron and (2) acts in supplying precursors of the organic matrix.[11] In *Acropora millepora* (symbiotic) ion transporters were not differentially expressed during the day or night and expression levels of genes associated with skeletal organic matrix were higher in light conditions.[12]

The day and night calcification has been also investigated in a-symbiotic corals, for which the absence of photosynthesis is not a prerequisite for calcification.[13,14] The calcification rate in *Tubastrea faulkneri* (a-symbiotic) was the same as the light-enhanced rate in *G. fascicularis* (symbiotic). This study proposed different mechanisms of calcification in two species, suggesting that the mineralization in the symbiotic coral was more "dark-repressed" than "light-enhanced".[15]

From these investigations we may infer that the enhancement of the calcification during the day, or repression during the night, could be a consequence of an increase in the OM synthesis and/or a higher $CaCO_3$ saturation state.

Recently, several experimental studies have suggested that the intra-skeletal OM components influence the $CaCO_3$ deposition; the control of the habit and composition of the precipitate is species specific, differs between symbiotic and a-symbiotic corals, and occurs in the presence of magnesium ions in the mineralization media.[16,17]

The study of the influence of the $CaCO_3$ saturation state at different OM concentrations on the precipitation of $CaCO_3$ in corals requires some preliminary considerations. The driving force for crystallization, both nucleation and growth, is the supersaturation, a practical measure of the chemical potential difference. Nucleation can start at supersaturation which is higher than a certain critical value, whereas crystal growth may occur at extremely low supersaturation and on already present crystal surfaces (crystal seed).[18,19] Biomineralization typically proceeds in a chemically complex environment and, besides the mineral constituent ions, a vast number of dissolved macromolecular and inorganic species, increased ionic strength and/or variable pH, as well different solid substrates influence this process and the properties of the solid phase. Many of the dissolved species (considered as the impurities with respect to crystallizing inorganic component) are known to be factors that substantially control polymorphism and physical-chemical properties during the crystallization process, such as Mg^{2+} or acidic macromolecules in the precipitation of $CaCO_3$.

Analysis of the precipitation (nucleation and crystal growth) kinetics can give insight into the mechanisms responsible for formation of specific solid phase and, besides the supersaturation, the presence of specific impurities has a major impact on polymorphism, morphology and size of the crystallites. However, simultaneous analysis of both processes is difficult, so a completely different experimental set up should be applied to obtain reliable information.

The main objective of this research was to investigate the influence of $CaCO_3$ supersaturation and concentration of soluble OM (SOM) extracted from symbiotic or a-symbiotic corals, on the kinetics of the deposition of $CaCO_3$ from artificial seawater (ASW), as well as to characterize the final products obtained in chemical systems that are representative of coral biomineralization in light and dark regimes.

Results

To achieve the objectives of this research, two ASW chemical systems were prepared: one with relatively high supersaturation with respect to aragonite ($S_a \approx 11$, ASW1), in which processes of homogeneous nucleation and growth take place simultaneously. This system is designed to mimic the high supersaturation conditions of coral calcification. In another system, the supersaturation was relatively low ($S_a \approx 5.8$, ASW2), which is similar to the low supersaturation conditions of coral's calcification. Under such conditions only the crystal growth, but not the homogeneous nucleation can take place. In the latter system the growth was initiated on well-defined aragonite crystal seeds, deliberately introduced to solution. In both systems, different concentrations of SOM, extracted from the symbiotic coral *B. europea* (SOM-Beu) and the a-symbiotic one *L. pruvoti* (SOM-Lpr) were added to investigate their effect on crystal growth or nucleation processes. Both corals are solitary species living in the Mediterranean Sea.[20,21]

Spontaneous precipitation of $CaCO_3$ in ASW1 system of higher supersaturation

The progress curves of spontaneous precipitation of $CaCO_3$, using the ASW1 system and respective SOM, seen as a change

of relative supersaturation and expressed with respect to aragonite equilibrium, $S_a \equiv ([a(Ca^{2+})\cdot a(CO_3^{2-})]/K_{sp})^{1/2}$, are shown in Figure 2. Precipitation was initiated by fast mixing of the reactants (carbonate and calcium containing solutions, with the addition of different concentrations of SOM-Beu or SOM-Lpr). The slopes of the respective curves are similar to the slope of the model system (no SOM addition) thus indicating that the kinetics of formation of solid phase(s) in each system are similar, irrespective of the type and the concentration of SOM. On the other hand, it could be seen that the precipitation in the model system, but also in the SOM-containing systems, started after a certain induction time, which increased with increasing SOM concentration. Thus, Figure 3 shows that the induction time increased almost linearly, from about 1000 s in the model systems to about 7000 s, or even 15000 s at the highest applied concentrations of SOM-Lpr or SOM-Beu, respectively. The X-ray diffraction pattern (Figures SI1 and SI2) analyses showed that using the ASW1 system, only aragonite precipitated, independently from the source and concentration of the SOM added.

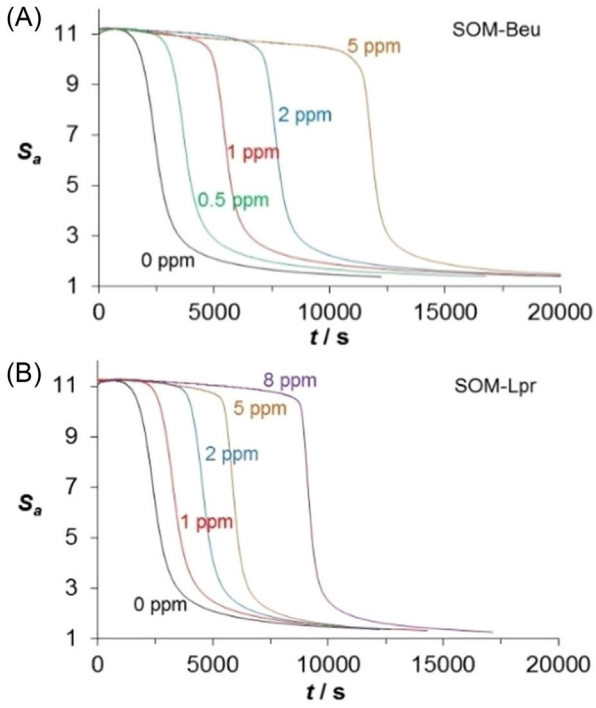

Figure 2. Progress curves, S_a versus time, in the system of higher initial supersaturation (ASW1, spontaneous precipitation) and in the presence of SOM-Beu (a) and SOM-Lpr (b). The respective concentrations of SOM are indicated: 0 ppm corresponds to the model system (no SOM addition).

At the same time, morphology and aggregation of aragonite particles spontaneously precipitated in the ASW1 system were investigated by scanning electron microscopy (Figure 4 and Figure SI4). It could be seen that the aragonite appeared in the form of aggregates, having a overall cauliflower shape (Figure 4A and SI4) in which clusters of nanoparticles with a preferential direction of association were observed (Figure 4C–H). In them no marked effect of SOMs were observed, except for

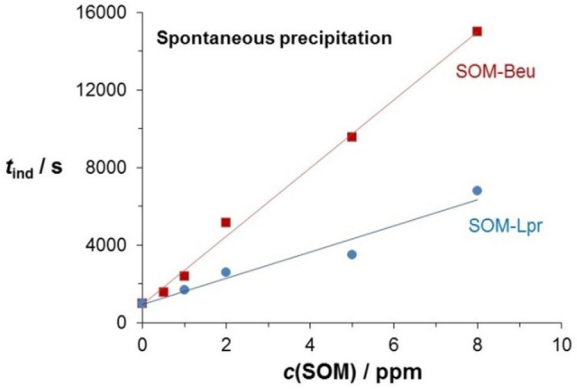

Figure 3. Induction time in the systems of spontaneous precipitation of the aragonite in the presence of different amounts of added SOM-Lpr and SOM-Beu.

samples obtained in the presence of the highest concentration of SOM in which a disordered association of nanoparticles seems to be present (Figure 4I,J). Such aggregation of particles is typical of aragonite precipitated from seawater,[22] but formation of similar shapes was observed in the presence of polyacrylic acid and also at high temperatures,[23] or in a case of electrodeposition on titanium foils and in the absence of any organic additives.[24] Detailed analysis of the aragonite aggregates showed that they are made of primary columnar particles of about 100 nm in length and about 30 nm thick. These primary particles were locally aligned along the columnar axis and showed rounded edges. The presence of a low concentration of SOM-Beu or SOM-Lpr, did not affect the overall shape of the aggregates and the features of the columnar building unites. On the other hand, at high concentration of SOMs (5.0 ppm SOM-Beu or 8.0 ppm SOM-Lpr) the crystal particles reduced in length to about 50 nm along the main axis. Indeed, size and morphology of the particles formed in the presence of higher concentrations of applied SOM show some similarity with the calcium carbonate particles observed in the EMZ of the coral skeleton (Figure 1C).

Seeding precipitation of $CaCO_3$ in the ASW2 system of lower supersaturation

The kinetics of crystal growth was determined by inoculation of a slightly supersaturated calcium carbonate solution, which mimics the chemical composition of typical seawater and contains one of the extracted macromolecules. Chemically and structurally pure crystals of aragonite, having a total surface of about 1.65 m^2 per dm^3 of solution, were used for inoculation (seeding) of the ASW2 solution in all experiments. Given that the supersaturation of the ASW2 solution was relatively low ($S_i \approx 5.8$, $pH_i \approx 8.9$), only the overgrowth of calcium carbonate on seed was obtained and no spontaneous precipitation occurred during the period of about 10000 s. The metastability of the solution was confirmed by preliminary experiments in which seed was not used. The experiments were also carried out in the presence of different concentrations of SOM-Lpr or SOM-Beu. The progress curves of the seeded precipitation experi-

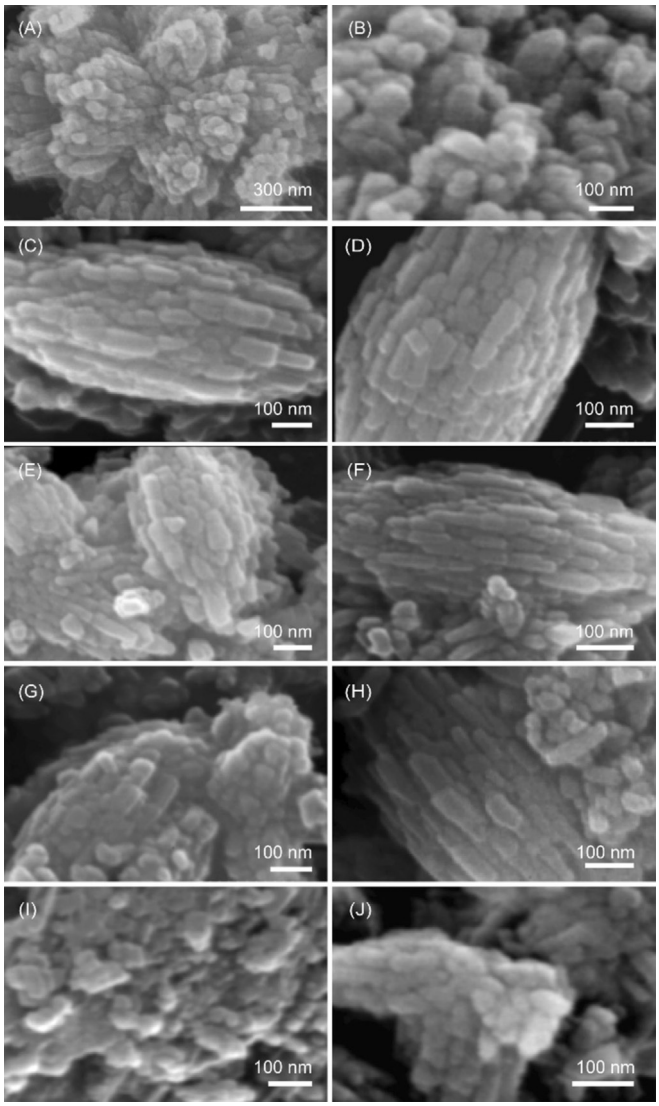

Figure 4. SEM images of aragonite particles spontaneously precipitated using the ASW1 system. (A and B) in the absence of SOM. (C, E, G, and I) in the presence of SOM-Beu at concentrations of 0.5 ppm (C), 1 ppm (E), 2 ppm (G) or 5.0 ppm (I). (D, F, H and J) in the presence of SOM-Lpr at concentrations of 1 ppm (D), 2 ppm (F), 5 ppm (H) or 8 ppm (J). The SEM images are representative of the entire population of particles. Additional SEM images are given in Figure SI4.

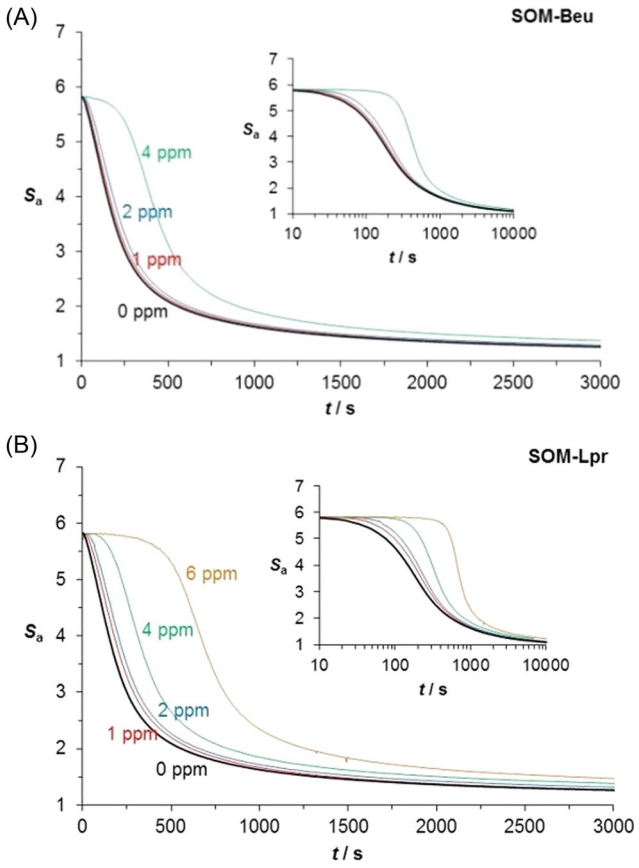

Figure 5. Progress curves, S_a versus time, of the seeded aragonite growth using the low-supersaturation systems, ASW2, in the presence of different concentrations of SOM-Beu (a) and SOM-Lpr (b). The numbers indicate concentrations of SOM applied. In the inset graphs, logarithmic time scales are shown.

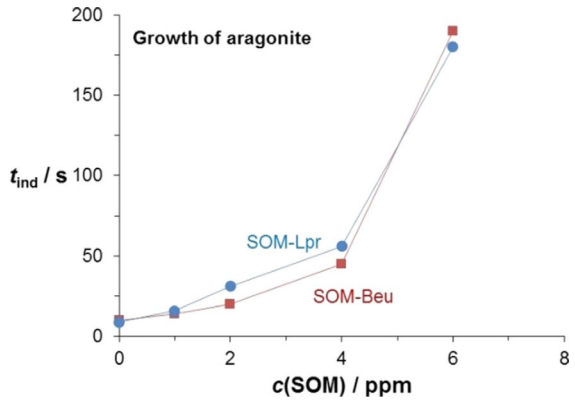

Figure 6. Induction time of precipitation in the seed growth of aragonite from the ASW2 system, in the presence of different concentrations of SOM-Beu and SOM-Lpr.

ments using the ASW2 system with the addition of SOM-Beu or SOM-Lpr are shown in the Figure 5. The kinetic curves show that precipitation started (seen as a lowering of supersaturation) after a certain induction time, t_{ind}, which increased with increasing concentration of each SOM. Thus, Figure 6 shows that induction time in the model systems is about 10 s, whereas at the highest applied concentrations of both SOM, measurable changes of supersaturation were obtained after about 180–190 s.

The identification of the mineral phase after termination of the inoculation experiments was based on FTIR spectroscopic analysis (Figure SI3) and only absorption bands of aragonite were detected.

The morphologies of the aragonite seed particles used in crystal growth experiments, as well as those obtained after the overgrowth in the pure system and in the presence of selected SOM are shown in Figure 7. The SEM images showed that the morphology of the aragonite that grow in the pure system

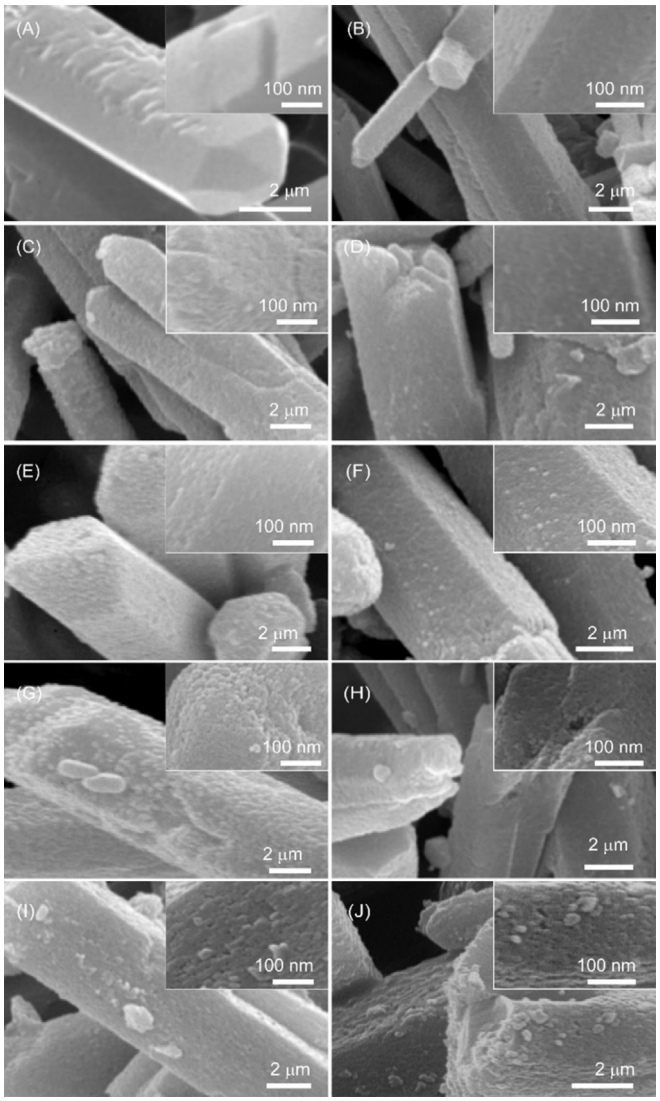

Figure 7. SEM images of the sample obtained in seeding experiments, using ASW2. (A) Aragonite seeds before and (B–J) after overgrowth. (B) In the absence of SOM (C, E, G, I) in the presence of SOM-Beu at concentrations of 1 ppm (C), 2 ppm (E), 4 ppm (G) or 6 ppm (I). (D, F, H, J) In the presence of SOM-Lpr at the concentration 1 ppm (D), 2 ppm (F), 4 ppm (H) or 6 ppm (J). The insets show higher magnification images of the seed surface after the aragonite deposition process. The illustrated micrographs are representative of the entire population of particles. Additional SEM images are reported in Figure SI5.

(Figure 7 A) and in the presence of low concentrations of SOMs are not significantly affected (Figure 7 C–F). However, at higher applied concentrations of SOMs, the surface roughness of the particles increased (Figure 7 G,H,J), whereas at 6 ppm SOM-Beu, even a textural reorganization of the particles was observed, as evidenced by the sharp edges of the overgrown particles (Figure 7 I and inset).

Analysis of the crystal growth kinetics

The growth rates of aragonite seed, $R \equiv dc/(dt \cdot A)$, presented as a function of relative supersaturation, S-1, obtained in the systems containing SOM-Beu and SOM-Lpr are shown in Figure 8.

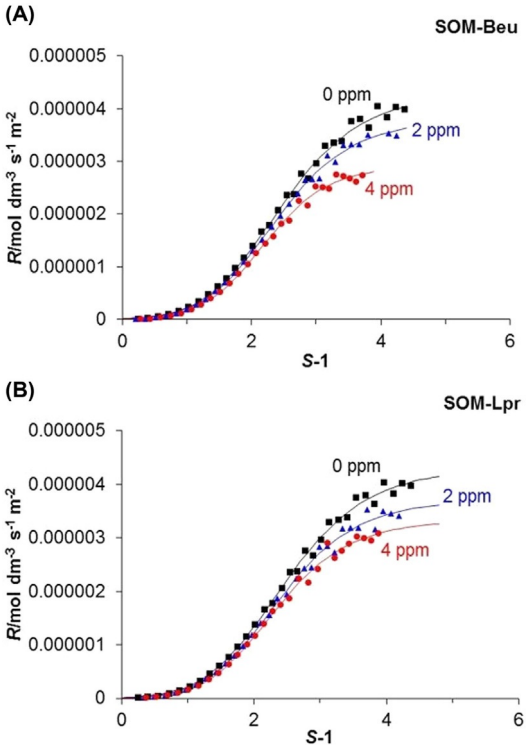

Figure 8. Representative growth rate curves of aragonite, shown as a function of supersaturation, in the ASW2 and different concentration of SOM from *B. europaea* (a) and *L. pruvoti* (b). The concentrations are indicated.

It is evident that only at higher supersaturations, which corresponds to the beginning of the process (Figure 5), do some difference between rates exist. The growth rates obtained after induction periods decrease with increasing concentration of SOM and the differences are slightly larger in the case of SOM-Beu. A dominant growth mechanism of aragonite crystals for a given range of supersaturations and SOM addition was determined by testing the respective growth rate models. Thus, two theoretical functions were tested: a) parabolic, $dc/dt = k_2\ c_{ppt}^{2/3}(S\text{-}1)^2$ and b) exponential rate law, $dc/dt = k_e S^{7/6}(S\text{-}1)^{2/3}(\ln S)^{1/6} \exp[-K_e/\ln S] k_e F(S) \exp[-K_e/\ln S]$.[18,19] The straight lines for the parabolic rate law (Figure 9) were obtained in referent system and in all systems containing SOM, indicating that, at given conditions, aragonite growth was controlled by a second-order surface reaction. This rate law points out that the growth predominantly proceeded on the spiral step emerging from the surface dislocation and, consequently, at extremely low supersaturation. Indeed, similar slopes have been obtained for all systems containing SOM and just a slight decrease of the rate constant at increasing addition of SOM has been observed. On the other hand, the absence of linearity for exponential law indicates that surface nucleation, which assumes higher supersaturation conditions, is not a relevant mechanism of aragonite growth under the given conditions. In Table 1 the kinetic parameters for crystal growth are shown: the parabolic rate constant, k_2, was calculated from the slope of the straight line for the parabolic test plot, whereas the rate order, n, was calculated from the logarithmic plot, R versus (S-1).

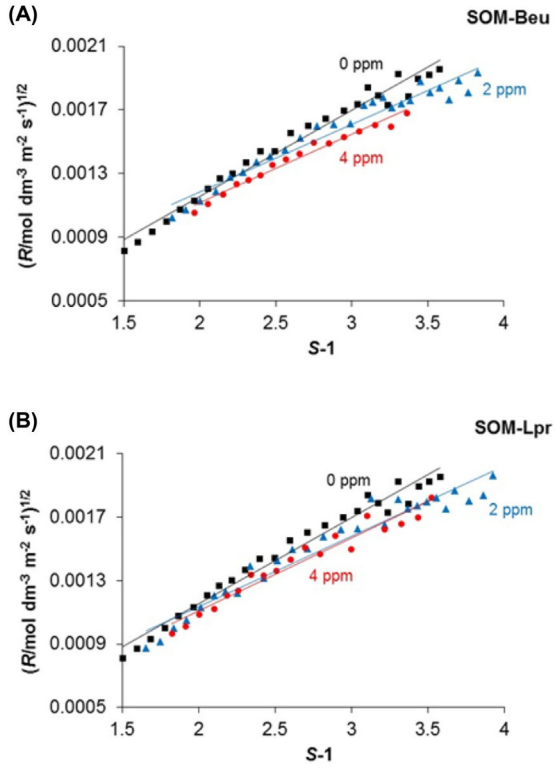

Figure 9. Typical test plots of the parabolic growth rate mechanism (growth on the spiral plane) of seeded growth of aragonite in the ASW2 and the range of initial supersaturations, $1 < S < 5$. The applied concentrations of SOM-Beu (a) and SOM-Lpr (b) are indicated.

Table 1. Kinetics parameters of seeded growth of aragonite in the ASW2 and the range of initial supersaturations, $1 < S < 5$, in the presence of different concentrations of SOM-Beu and SOM-Lpr. Rate order, n, is calculated from the logarithmic plot R versus (S-1) and rate constant, k_2, by testing the parabolic growth rate law.

SOM	c [ppm]	n	t_{ind} [s]	k_2 [μmol dm^{-3} s^{-1} m^{-2}]
	0	2.24	10	0.29
Beu	1	2.23	14	0.24
	2	2.311	20	0.18
	4	2.47	45	0.18
	6	–	190	–
Lpr	1	2.27	16	0.24
	2	2.31	31	0.20
	4	2.48	56	0.21
	6	–	180	–

Discussion

Several investigations on the role of SOM from different coral species in the polymorphic precipitation of $CaCO_3$ have been reported,[16,25–28] but, to our knowledge, the effect of SOMs on kinetic and thermodynamic precipitation parameters of aragonite have not been analyzed. This work covers that lack of information with a comparative in vitro study of the influence of SOMs from *B. europea* and *L. pruvoti* on the kinetics of precipitation of aragonite. The aragonite was precipitated in ASW, which closely mimics the sea water media from which the deposition of aragonite in corals takes place.[17,29–31] Experiments were carried out by setting either the higher supersaturation conditions that enable spontaneous precipitation of new crystals, or lower supersaturations that enable only crystal growth on already present aragonite seed. Indeed, the applied experimental set ups may be relevant for the understanding of day and night calcification of corals, which correlates to higher or lower supersaturation conditions, respectively.

The values of supersaturations applied in this work are based on published data, which are appropriately adjusted for specific experimental conditions and a requirement to discriminate the effects caused, either exclusively by nucleation or crystal growth processes. Thus, by applying a very high value of supersaturation, like that reported for day calcification in *G. fascicularis* ($S_a = 25$),[10] a rapid and massive spontaneous precipitation was obtained in preliminary experiments, so the effects of the SOM were difficult to detect. On the other hand, when lower supersaturation conditions were applied, like that reported for *G. fascicularis* ($S_a = 3$),[10] extremely slow growth on aragonite seed prevented reproducible kinetics analysis. Therefore, higher supersaturation used in this work, $S_a \approx 11$, was found to be optimal for analysis of the nucleation period of the precipitation in the presence of SOM. In addition, the value is supported by the reported data for the supersaturation conditions of the coral species *Porites sp.* ($S_a \approx 12 \pm 2$), as estimated by Raman spectroscopy.[32] On the other hand, supersaturation used in crystal growth experiments, $S_a \approx 5.8$, was low enough to exclude any spontaneous precipitation process, but high enough to produce a detectable precipitation of material, even in the presence of SOM.

As a source of SOM, symbiotic and a-symbiotic coral species were used, which allowed the features related to the daytime photosynthetic activities of the organism to be highlighted. The content of SOM extracted from *B. europaea* was higher than in *L. pruvoti*,[16,33] whereas their amino acid compositions were almost identical.

The rationalization of the data obtained from the precipitation experiments of aragonite from chemically complex model systems such as ASW is difficult, and among the other parameters relevant for precipitation, the presence of SOMs is certainly the most intriguing. This is due to numerous interactions that may occur at the crystal-solution interfaces. Indeed, the adsorption of the additives (i.e., SOMs) on crystal surfaces may affect thermodynamic and kinetic terms relevant for growth, but also the solubility of crystals.[18,34,35] The adsorption of SOMs, or any foreign molecules, on a crystal surface decreases its interfacial energy, γ (a thermodynamic parameter), which may cause an increase of nucleation rate (promotion of nucleation), but also decrease the radius of the critical two-dimensional surface nucleus, which effectively increases the growth rate. On the other hand, additives adsorbed on the surface or at the kink positions at the step, decrease the motion of the growing steps (kinetic parameter), which is exactly opposite to thermodynamic effect. Although it is difficult to predict the

overall effect of additives on crystallization, there is extensive experimental evidence that, at low supersaturation, the growth rate can be increased in the presence of low additive concentrations, while at higher concentrations the retardation of the kinetics may be the dominant effect.[18,34,36] The additives present at low concentrations have only minor effects on the solubility of the solid phase and can be neglected in the systems similar to those described in this study. However, the mechanism and extent of interactions between specific additive and preferential adsorption sites at the crystal surface can strongly affect the mobility of the molecules. Consequently, in the extreme case, molecules can be either predominantly adsorbed at the terraces (immobile additives) or at the kink position on growing steps (mobile additives). In view of the above dichotomy, it is clear that a straightforward interpretation of the crystal growth kinetic data, obtained in the systems containing several additives is particularly difficult in ASW that contains a high concentration of Mg^{2+}, strong $CaCO_3$ growth inhibitor, and increased ionic strength. In this study, SOM/aragonite interactions in precipitation experiments are perceived either as inhibition (i.e., extension of induction period) or growth rate changes with respect to the reference. A specific characteristic of the systems of aragonite crystals and SOM dissolved in ASW, is well defined induction time which increases with increasing SOM concentration. In addition, subsequent precipitation (growth) kinetics was found to be similar to properties of the referent system and no significant inhibition was observed. Such findings can indicate a significant and almost complete incorporation of available macromolecules into the mineral phase during the induction period and subsequent growth of crystals which is only slightly disturbed. The proposed mechanism is significantly different from similar systems described in the literature, in which calcite growth in the presence of synthetic polypeptides (poly-L-aspartic and poly-L-glutamic acid, poly-L-lysine) has been analyzed. In those systems, in which only one additive was present, no induction time was observed, as well as continuous inhibition and complete termination of growth at critical supersaturation.[35,37] For comparison purposes, the growth of calcite crystals under similar conditions to those applied in this work (ASW, supersaturation, pH, seed and SOM concentration) was also analyzed and it was found to follow a pattern similar to previously described synthetic polypeptide/calcite systems. In this case, no induction time was observed, the growth was controlled by surface nucleation and SOM significantly reduced the kinetics (Figure SI6). Nevertheless, it should be considered that the calcite interactions with ASW are specific and are influenced by the presence of a high concentration of Mg^{2+}, which is a strong calcite growth inhibitor. In contrast, the interactions of aragonite with Mg^{2+} are less pronounced, which makes a principle difference between the behavior of the twopolymorphs.

The kinetics data for aragonite obtained in this study clearly show that the presence of SOM inhibits the precipitation. Such inhibition has been observed as a systematic increase of induction period with increasing SOM addition, which occurred during both the nucleation and growth periods. The inhibition activity of SOM-Beu is evidently stronger than that of SOM-Lpr, which may imply a higher supersaturation level in the mineralization site in *B. europaea* than in *L. pruvoti*. This is consistent with findings reported for *Acropora sp.*, in which the activity of ion transporters is not affected by the light conditions, so higher ion concentration could be achieved in a longer time.[12] For the systems described in this work, the effect could be enhanced by the higher skeletal content of SOM in *B. europaea*, with respect to *L. pruvoti*.[16]

The analyses of the in vitro kinetics data obtained at low supersaturation (Table 1, Figure 8) show that the growth mechanism of aragonite, after the respective induction time, is not significantly affected by the presence of either SOM-Beu or SOM-Lpr and occurs by integration of growth units of $CaCO_3$ into the spiral steps, as reported previously.[38] At high supersaturation, the shape and aggregation of the crystallites are minimally affected by the presence of either SOM-Beu or SOM-Lpr. Only when SOMs were present at the highest concentration was a reduction of aragonite column length observed, generating spheroidal particles that may resemble those observed in the EMZs of coral skeletons.[6,7] The latter observation implies that the SOM interacts, and stabilizes, crystalline planes perpendicular to the main axis (i.e., the *c* axis). Such interaction has not been previously reported for coral SOM macromolecules, but has been widely observed in mollusk shell during the formation of the nacre.[39] These observations may match with the concepts that deposition of calcium carbonate particles in the EMZs occurs at high supersaturations,[40] as well as that the OM plays an important role in controlling the shape and aggregation of the particles. Therefore, it may be concluded that the presence of the OM in the coral skeleton cannot be only the result of a physical entrapment.[41]

At low supersaturation and in the presence of SOM, only the crystal growth process occurs and, after the well-defined induction time, no significant changes of kinetics or mechanisms of mineralization could be observed. Actually, the increasing SOM concentration progressively affects the morphology of the original aragonite particles, as illustrated by SEM images. The presence of specific textures of the overgrown aragonite is observed in the presence of 6 ppm SOM-Beu, suggesting a capability of SOM molecules to assemble aragonite crystalline units. This specificity in the interaction of SOM with the aragonite seed is additionally evidenced by the fact that, when calcite was used as a seed, magnesium calcite precipitated under the same experimental conditions.

The obtained knowledge may imply that coral calcification under low supersaturation conditions may occur by deposition on previously formed aragonite crystals, which could take place mainly on the FZs. On the other hand, at high supersaturation the formation of aragonite particles does not require the presence of seeds, and, consequently, the growth of both EMZs and FZs is likely. According to the obtained results, and considering the two-step model of growth,[6] as well as some recent observations on coral biomineralization,[42] it can be speculated that the activities of different cells and macromolecules are involved in the formation of the EMZs and FZs.

Conclusion

This research provides kinetic and thermodynamic data of aragonite precipitation in vitro from ASW at different supersaturations in the presence of SOM from a symbiotic (photosynthetic) and a-symbiotic coral. The knowledge gained from kinetic and thermodynamic data analyses, as well as the microscopic observations can be summarized:

1. Under high supersaturation conditions, a significant and almost complete incorporation of available macromolecules into the mineral phase during the nucleation and subsequent growth of crystals occurs. SOMs incorporate in aragonite, but not in calcite crystals under similar conditions. The precipitated aragonite appears as aggregates of nanoparticles resembling those observed in the EMZs.
2. The inhibition of precipitation can be observed as a systematic increase of induction period with increasing SOM addition, which occurs during both the nucleation and crystal growth stages, corresponding to high supersaturation and low supersaturation conditions, respectively.
3. The growth mechanism of aragonite obtained by seeding experiments (growth on the spiral step), did not change after the addition of SOM. However, the presence of high concentration of SOMs induces a change in the morphology and shape of the growing crystalline units.
4. The inhibition activity of SOM-Beu is stronger than that of SOM-Lpr.

Finally, the above conclusions may indicate that the calcification of corals is controlled by both a pure physiochemical mechanism, according to which physiological parameters control only the saturation state of the precipitating fluid, and a mechanism based on the two-step mode of growth, according to which the SOM plays an active role in the process.

Experimental Section

The soluble organic matrix from *B. europea* (SOM-Beu) or *L. pruvoti* (SOM-Lpr) was extracted as reported elsewhere.[43] The chemicals used to prepare the reactant solutions, $CaCl_2$, Na_2CO_3, $NaHCO_3$, $MgCl_2$, and NaCl, were analytical grade and the deionized water was of high quality (conductivity $<0.055\ \mu S\,cm^{-1}$). As a precipitation model, artificial seawater, ASW, was used,[44] with the composition: $c(Na_2CO_3)+c(NaHCO_3)=5\times10^{-3}\ mol\,dm^{-3}$, $c(CaCl_2)=0.01\ mol\,dm^{-3}$, $c(MgCl_2)=0.05\ mol\,dm^{-3}$ and $c(NaCl)=0.3\ mol\,dm^{-3}$. The pH was pre-adjusted by the appropriate addition of HCl or NaOH or/and by varying the $Na_2CO_3/NaHCO_3$ ratio. The systems that were used in spontaneous precipitation experiments have higher initial supersaturation, ASW1 ($pH_i\approx10.2$, $S_a\approx11$). Seeding experiments were performed in a system with lower initial supersaturation, ASW2 ($pH_i\approx8.9$; $S_a\approx5.8$). Experiments were carried out in a thermostated double-walled glass vessel of 20 cm^3 capacity, at a constant temperature of 21 °C. The systems were continuously stirred at a constant rate by means of a Teflon-coated magnetic stirring bar. In each of the systems the precipitation was initiated by pouring 10 cm^3 of calcium containing solution into 10 cm^3 of carbonate containing solution. The anionic solution contained Na_2CO_3, $NaHCO_3$, and NaCl, while the cationic solution was made up of $CaCl_2$, $MgCl_2$, and NaCl. When needed, SOM-Beu or SOM-Lpr, was added into the carbonate solution. The concentrations of biomacromolecules used in experiments varied in the range $0.5\ ppm\le c_i(SOM\text{-}Beu)\le8\ ppm$ and $1\ ppm\le c_i(SOM\text{-}Lpr)\le8\ ppm$. The systems used as reference contained the same initial reactant concentrations and volumes, but without SOM-Beu or SOM-Lpr. During the experiments the reaction vessel was tightly closed with a Teflon cover, thus minimizing the exchange of carbon dioxide between the air and the reaction system. The use of a closed system, without any atmosphere above the solution, enables strict control of pH and the supersaturation. The progress of the precipitation process was followed by measuring the change of pH with time, using a combined glass-calomel electrode (GK 2401C) connected to a digital pH meter (PHM 290, Radiometer). From the measured H^+ activity and the known total initial charge and mass balance of calcium chloride and sodium carbonate, the initial concentrations and activities of the relevant ionic species have been calculated. The precipitated calcium carbonate concentration, c_{ppt}, was determined by subtracting the calculated total concentration of calcium or carbonate species in the closed system, from the known initial concentrations of calcium chloride or sodium carbonate. The crystal growth rate, R, was calculated by numerical differentiation of the total dissolved calcium concentration as a function of time, t, and normalized with respect to the surface area of the precipitate, A, at a particular moment: $R=-dCa_{tot}/(dt\cdot A)$. During the crystal growth, the total surface area of seed increased and was calculated by using the data for the corresponding molar concentration of precipitated total calcium carbonate, c_{ppt} ($mol\,dm^{-3}$). Details of the calculation can be found in previous publications.[34,45–49] Samples of precipitate used for the analyses were taken at the end of each experiment, when the total volume of suspension was filtered through a 0.22 μm membrane filter. The precipitate was washed with small portions of water and dried at 50 °C. The mineralogical composition of the dried samples was analyzed by FTIR spectroscopy and by X-ray powder diffraction. Fourier transform infrared (FTIR) spectra of samples in KBr disks were collected at room temperature with a FTIR Nicolet 380 Thermo Electron Corporation or Tensor II, Bruker spectrophotometer, working in the 400–4000 cm^{-1} wavelength range at a resolution of 2 cm^{-1}. A finely ground, approximately 1 wt.% mixture of the sample in KBr, was pressed into a transparent disk using a hydraulic press and applying a pressure of 48.6 psi. X-ray powder diffraction analyses were performed using an X'Celerator detector fitted on a PANalytical X'Pert Pro diffractometer, using Cu Kα radiation generated at 40 kV and 40 mA. The data were collected within the 2θ range from 10° to 60° with a step size (Δ2θ) of 0.02° and a counting time of 1200 s. Fixed anti-scatter and divergence slits of 1/2° were used with 10 mm beam mask and all scans were carried out in "continuous" mode. The morphology of the crystals was observed by light microscopy and by scanning electron microscopy (FEG SEM Hitachi 6400 and Phenom model G2). The specific surface area was determined by the multiple BET method (Micromeritics, Gemini), using liquid nitrogen.

Acknowledgements

This work was supported by a grant from the European Research Council (FP7/2007-2013)/ERC Grant Agreement No. [249930] and was supported in part (B.N.D., D.K.) by the Croatian Science Foundation under the project (IP-2013-11-5055) and Unity through Knowledge Fund grant. G.F. and S.F. thank

the Consorzio Interuniversitario di Ricerca per la Chimica die Metalli nei Sistemi Biologici (CIRCMSB) for their support.

Conflict of interest

The authors declare no conflict of interest.

Keywords: aragonite · biomineralization · corals · kinetics · supersaturation

[1] M. D. Spalding, C. Ravilious, E. P. Green, *World Atlas of Coral Reefs*, University of California Press, Berkeley, **2001**.
[2] A. L. Cohen, T. L. McConnaughey, *Rev. Mineral. Geochemistry* **2003**, *54*, 151 – 187.
[3] J.-P. Gattuso, D. Allemand, M. Frankignoulle, *Am. Zool.* **1999**, *39*, 160 – 183.
[4] A. A. Venn, E. Tambutte, M. Holcomb, J. Laurent, D. Allemand, S. Tambutte, *Proc. Natl. Acad. Sci. USA* **2013**, *110*, 1634 – 1639.
[5] J.-P. Cuif, G. Lecointre, C. Perrin, A. Tillier, S. Tillier, *Zool. Scr.* **2003**, *32*, 459 – 473.
[6] J.-P. Cuif, Y. Dauphin, *J. Struct. Biol.* **2005**, *150*, 319 – 331.
[7] J.-P. Cuif, Y. Dauphin, J. Doucet, M. Salome, J. Susini, *Geochim. Cosmochim. Acta* **2003**, *67*, 75 – 83.
[8] S. Weiner, L. Addadi, *Annu. Rev. Mater. Res.* **2011**, *41*, 21 – 40.
[9] J. H. Vandermeulen, N. D. Davis, L. Muscatine, *Mar. Biol.* **1972**, *16*, 185 – 191.
[10] F. A. Al-Horani, S. M. Al-Moghrabi, D. de Beer, *Mar. Biol.* **2003**, *142*, 419 – 426.
[11] A. Moya, S. Tambutté, A. Bertucci, E. Tambutté, S. Lotto, D. Vullo, C. T. Supuran, D. Allemand, D. Zoccola, *J. Biol. Chem.* **2008**, *283*, 25475 – 25484.
[12] A. Bertucci, S. Forêt, E. E. Ball, D. J. Miller, *Mol. Ecol.* **2015**, *24*, 4489 – 4504.
[13] T. G. Jacques, M. E. Q. Pilson, *Mar. Biol.* **1980**, *60*, 167 – 178.
[14] T. G. Jacques, N. Marshall, M. E. Q. Pilson, *Mar. Biol.* **1983**, *76*, 135 – 148.
[15] A. Moya, S. Tambutté, E. Tambutté, D. Zoccola, N. Caminiti, D. Allemand, *J. Exp. Biol.* **2006**, *209*, 3413 – 3419.
[16] G. Falini, S. Fermani, S. Goffredo, *Semin. Cell Dev. Biol.* **2015**, *46*, 17 – 26.
[17] T. Mass, A. J. Giuffre, C.-Y. Sun, C. A. Stifler, M. J. Frazier, M. Neder, N. Tamura, C. V. Stan, M. A. Marcus, P. U. P. A. Gilbert, *Proc. Natl. Acad. Sci. U.S.A.* **2017**, *114*, E7670 – E7678.
[18] J. J. De Yoreo, P. G. Vekilov, *Rev. Mineral. Geochemistry* **2003**, *54*, 57 – 93.
[19] L. Brečević, D. Kralj in *Surfactant Science Series, Vol. 88* (Ed.: N. Kallay), Marcel Dekker, New York, **2000**; pp. 435 – 474.
[20] S. Goffredo, G. Mattioli, F. Zaccanti, *Coral Reefs* **2004**, *23*, 433 – 443.
[21] E. Caroselli, F. Zaccanti, G. Mattioli, G. Falini, O. Levy, Z. Dubinsky, S. Goffredo, *PLoS One* **2012**, *7*, e37848.
[22] A. Juillet-Leclerc, S. Reynaud, C. Rollion-Bard, J. P. Cuif, Y. Dauphin, D. Blamart, C. Ferrier-Pagès, D. Allemand, *Geochim. Cosmochim. Acta* **2009**, *73*, 5320 – 5332.
[23] S. Ouhenia, D. Chateigner, M. A. Belkhira, E. Guilmeau, C. Krauss, *J. Cryst. Growth* **2008**, *310*, 2832 – 2841.
[24] C. Krauss, D. Chateigner, O. Gil, *Cryst. Growth Des.* **2008**, *8*, 4378 – 4382.
[25] D. Allemand, É. Tambutté, J.-P. Girard, J. Jaubert, *J. Exp. Biol.* **1998**, *201*, 2001 – 2009.
[26] D. Allemand, É. Tambutté, D. Zoccola, S. Tambutté " *Coral Calcification" in Cells to Reefs (Coral Reefs: An Ecosystem in Transition* (Ed.: Z. Dubinsky, N. Stambler), Springer, Dordrecht, **2011**, pp. 119 – 150.
[27] J. L. Drake, T. Mass, L. Haramaty, E. Zelzion, D. Bhattacharya, P. G. Falkowski, *Proc. Natl. Acad. Sci. USA* **2013**, *110*, 3788 – 3793.
[28] P. Ramos-Silva, J. Kaandorp, L. Huisman, B. Marie, I. Zanella-Cléon, N. Guichard, D. J. Miller, F. Marin, *Mol. Biol. Evol.* **2013**, *30*, 2099 – 2112.
[29] C.-Y. Sun, M. A. Marcus, M. J. Frazier, A. J. Giuffre, T. Mass, P. U. P. A. Gilbert, *ACS Nano* **2017**, *11*, 6612 – 6622.
[30] A. Akiva, M. Neder, K. Kahil, R. Gavriel, I. Pinkas, G. Goobes, T. Mass, *Nat. Commun.* **2018**, *9*, 1880.
[31] R. Gavriel, M. Nadav-Tsubery, Y. Glick, A. Yarmolenko, R. Kofman, K. Keinan-Adamsky, A. Berman, T. Mass, G. Goobes, *Adv. Funct. Mater.* **2018**, *28*, 1707321.
[32] T. M. DeCarlo, J. P. D'Olivo, T. Foster, M. Holcomb, T. Becker, M. T. McCulloch, *Biogeosciences* **2017**, *14*, 5253 – 5269.
[33] A. Adamiano, S. Goffredo, Z. Dubinsky, O. Levy, S. Fermani, D. Fabbri, G. Falini, *Anal. Bioanal. Chem.* **2014**, *406*, 6021 – 6033.
[34] B. Njegić-Džakula, L. Brečević, G. Falini, D. Kralj, *Cryst. Growth Des.* **2009**, *9*, 2425 – 2434.
[35] K. Sangwal, *Prog. Cryst. Growth Charact. Mater.* **1996**, *32*, 3 – 43.
[36] B. Njegić-Džakula, G. Falini, L. Brečević, Ž. Skoko, D. Kralj, *J. Colloid Interface Sci.* **2010**, *343*, 553 – 563.
[37] K. Sangwal, *J. Cryst. Growth* **1993**, *128*, 1236 – 1244.
[38] A. J. Gratz, P. E. Hillner, P. K. Hansma, *Geochim. Cosmochim. Acta* **1993**, *57*, 491 – 495.
[39] M. Suzuki, K. Saruwatari, T. Kogure, Y. Yamamoto, T. Nishimura, T. Kato, H. Nagasawa, *Science* **2009**, *325*, 1388 – 1390.
[40] D. J. Barnes, *Science* **1970**, *170*, 1305 – 1308.
[41] M. Holcomb, A. L. Cohen, R. I. Gabitov, J. L. Hutter, *Geochim. Cosmochim. Acta* **2009**, *73*, 4166 – 4179.
[42] T. M. DeCarlo, S. Comeau, C. E. Cornwall, M. T. McCulloch, *Proc. R. Soc. B* **2018**, *285*, 20180564.
[43] S. Goffredo, P. Vergni, M. Reggi, E. Caroselli, F. Sparla, O. Levy, Z. Dubinsky, G. Falini, *PLoS One* **2011**, *6*, e22338.
[44] S. L. Tracy, C. J. P. François, H. M. Jennings, *J. Cryst. Growth* **1998**, *193*, 374 – 381.
[45] D. Kralj, J. Kontrec, L. Brečević, G. Falini, V. Nöthig-Laslo, *Chem. Eur. J.* **2004**, *10*, 1647 – 1656.
[46] D. Kralj, L. Brečević, J. Kontrec, *J. Cryst. Growth* **1997**, *177*, 248 – 257.
[47] D. Kralj, L. Brečević, A. E. Nielsen, *J. Cryst. Growth* **1990**, *104*, 793 – 800.
[48] D. Kralj, L. Brečević, A. E. Nielsen, *J. Cryst. Growth* **1994**, *143*, 269 – 276.
[49] D. Kralj, L. Brečević, *Colloids Surf. A* **1995**, *96*, 287 – 293.

Manuscript received: February 13, 2019
Accepted manuscript online: March 6, 2019
Version of record online: April 26, 2019